IEEE Access
Multidisciplinary | Rapid Review | Open Access Journal

Received December 4, 2018, accepted January 29, 2019, date of publication February 13, 2019, date of current version March 7, 2019.

Digital Object Identifier 10.1109/ACCESS.2019.2898983

Time Diversity Passive Time Reversal for Underwater Acoustic Communications

SALMAN I. SIDDIQUI AND HEFENG DONG, (Member, IEEE)
Department of Electronic Systems, Norwegian University of Science and Technology, 7491 Trondheim, Norway
Corresponding author: Salman I. Siddiqui (salman.siddiqui@ntnu.no)

ABSTRACT Underwater acoustic signal propagation is greatly affected by source-receiver motion, surface variations, and water column variabilities, which make the underwater acoustic communications very challenging. A passive time reversal (pTR) system is widely used for underwater communication systems due to its focusing property, which minimizes the time spreading of the underwater channel. The performance of the pTR system degrades when the underwater channel varies rapidly. During the experiment in TrondheimFjord on September 22, 2016, some environmental variations are observed which resulted in channel variations and the performance of the pTR system degraded. A time diversity pTR system is proposed and it uses the time diversity of the channel to compensate for the channel variations. The proposed system is tested at two receiver positions and it provides 2–3-dB gain in terms of mean square error in the presence of rapid channel variations.

INDEX TERMS Underwater acoustics, underwater communication, time reversal.

I. INTRODUCTION

Underwater acoustic communications is a challenging field of research due to adverse environmental effects of the underwater channel. The underwater channel is a bounded medium which induces time as well as frequency spreading in the received signal. The time spreading is due to different replicas of the received signal with different delays, including the direct arrival and surface and/or bottom reflected arrivals. The frequency spreading is due to the environmental variations such as source and/or receiver motion, surface variations and water column variations.

The time reversal (TR) communication system has gained a lot of attention for underwater communications. The TR system provides low complexity, and its focusing capabilities make it very favorable for underwater communication applications [1]–[3]. In the TR system, the received signal is correlated with the time-reversed version of the estimated impulse response (IR) of the channel. A probe signal is transmitted before the data signal for channel IR estimation. The IR estimate is then used as a synthetic channel for the temporal focusing of the data signal. This is equivalent to the deconvolution of the multipath generated by the real channel.

The time spreading of the underwater channel affects the focusing of the pTR system by inducing intersymbolic interference (ISI) which degrades the performance of the communication system [4], [5]. The pTR system tries to compensate for the channel multipath but it is very sensitive to the underwater channel variations. The performance of pTR system in the presence of channel variations was studied in [6] and shown that performance degrades significantly in the presence of the rapid environmental variations. Different solutions for combating the ISI in the pTR system were presented in [7]. In addition to the time spreading, the received signal also spreads in the frequency domain due to surface motion and source and/or receiver motion. These variations also affect the focusing of the pTR system. Different channel tracking techniques are proposed in the literature to compensate for the frequency spreading. A channel tracker was combined with the linear decoder for Doppler spread compensation [8], [9]. A continuous channel update and Doppler tracking were introduced before the TR operation to compensate for the time variability [10]. A frequency shift pTR (FSpTR) was proposed in [11] which applies a frequency shift to the channel IR estimate to compensate for the frequency spreading. A decision feedback equalizer (DFE) was combined with the pTR to improve the performance of the communication system [12].

In the underwater environment, the transmitted signal reaches the receiver through multiple paths. Each of the arrivals is affected by the environmental factors in a different manner which induces different Doppler in each arrival [13].

The associate editor coordinating the review of this manuscript and approving it for publication was Abdul Wahid.

2169-3536 © 2019 IEEE. Translations and content mining are permitted for academic research only.
Personal use is also permitted, but republication/redistribution requires IEEE permission.
See http://www.ieee.org/publications_standards/publications/rights/index.html for more information.

In most of the Doppler compensation techniques, the Doppler effect was compensated by a single value which did not provide the optimal compensation. A path specific Doppler compensation technique was proposed in [14] where each path was isolated using the delay-sum beamformer and compensated separately. In case of fewer receivers, it is impossible to isolate different arrivals with the delay-sum beamformer.

In this work, an improved pTR system named time diversity pTR (TDpTR) system is proposed. It uses the time diversity of the underwater channel to compensate for the environmental variations. In the conventional pTR systems, the single probe signal is used for channel IR estimation. In this work, multiple probe signals are transmitted to obtain different channel IR estimates and the optimal channel IR is selected to compensate for the environmental effects. The proposed TDpTR system is tested by the real data collected during the sea trial on 22 September 2016 in TrondheimFjord. Different acoustic signals were transmitted including chirp signals and binary phase shift keying (BPSK) modulated signals. Strong channel variations are observed during the acoustic transmissions which degrade the performance of the communication system. The TDpTR system compensates for the channel variations and provides 2-3 dB gain in terms of mean square error (MSE) and 20-30 % gain in terms of bit error rate (BER). It is also shown that each receiver is affected by different channel variations and the optimal performance is achieved by compensating each receiver separately.

The paper is organized as follows: Section II describes the experiment. Section III gives the theoretical background. The mathematical formulation of the proposed technique is provided in section IV. Section V explains the implementation of the TDpTR system. The results and observations are presented in section VI. Section VII concludes the paper.

II. EXPERIMENTAL SETUP AND DATA COLLECTION

The data presented in this paper were obtained during an experiment on 22 September 2016 in TrondheimFjord. Fig. 1 shows the bathymetric map of the area and the locations of the source (position B) and the receivers (positions C and D). The source was deployed at 20 m depth and the water depth at the source position was 150 m. The source signal was transmitted from the transmitter deployed on the NTNU research vessel R/V Gunnerus. Four autonomous hydrophones were deployed at two positions C and D. At each position, two hydrophones were deployed at 30 m and 60 m depths, respectively. The water depths at C and D were 200 m and 100 m, respectively. The source-receiver range at positions C and D were 480 m and 670 m, respectively. Fig. 2 shows the sound speed profiles (SSPs) at both source and receiver positions. The SSPs were collected at two different times at each position. Due to the shape of the SSPs and the source depth, the acoustic signals propagate towards both the surface and the bottom.

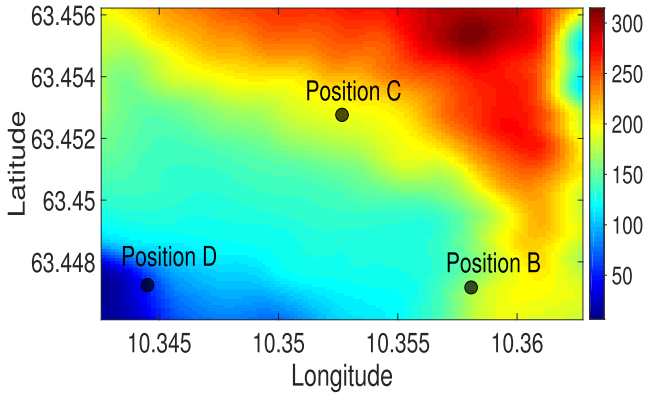

FIGURE 1. Bathymetry diagram of the experiment site. The source is located at position B, and the receivers are located at positions C and D, respectively. The water depths at positions B, C and D were 150 m, 100 m, and 200 m, respectively. The source-receiver ranges at positions C and D were 480 m and 670 m, respectively.

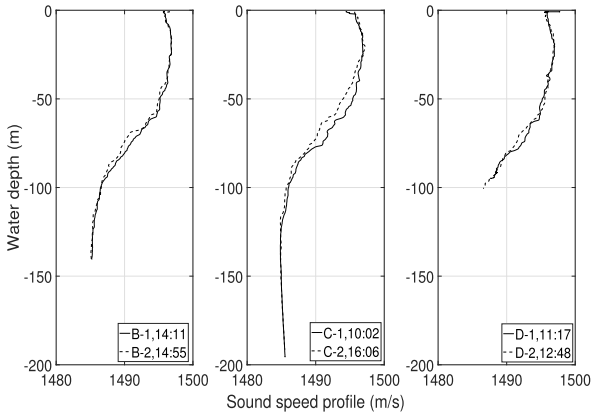

FIGURE 2. SSPs collected at positions B (left panel), C (middle panel) and D (right panel). At each position, two SSPs were collected. At positions B, C and D SSPs were collected at 14:11 and 14:55, 10:02 and 16:06 and 11:17 and 12:48, respectively. The SSPs are marked according to the time of acquisition.

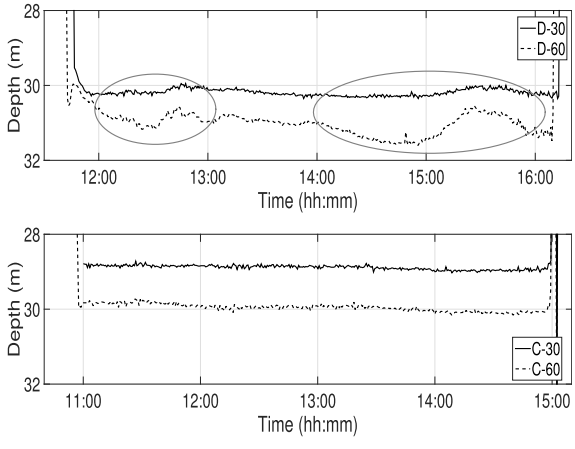

FIGURE 3. Sensor data showing the receiver depths during the measurement time. Solid and dashed lines represent the depth data for receivers at 30 m and 60 m at position D (top panel) and position C (bottom panel), respectively. The depth data of 60 m receiver are shifted for comparison. The ellipsed region shows the periodic depth variations at position D between 12:00 to 13:00 and 14:00 to 16:00, respectively.

All the receivers were equipped with a sensor which collects the temperature and pressure data. Fig. 3 shows the depth data obtained from the sensor at position D (top panel)

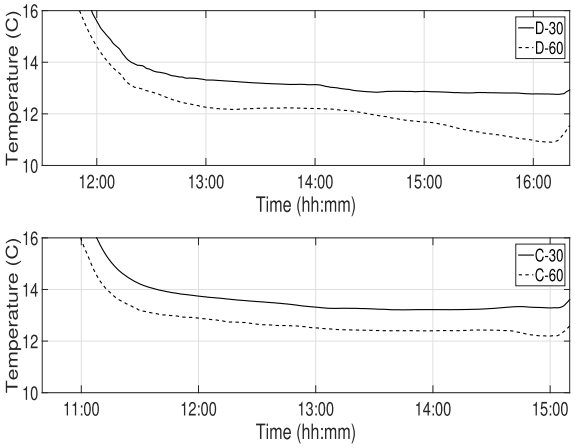

FIGURE 4. Sensor data showing the water temperature during the measurement time. Solid and dashed lines represent the temperature data for receivers at 30 m and 60 m at position D (top panel) and position C (bottom panel), respectively.

and position C (bottom panel) during the measurement time. Solid and dashed lines represent the depth data for receivers at 30 m and 60 m, respectively. The depth data from the receiver at 60 m depth are shifted by 26 m and 30 m at positions D and C, respectively. The x-axis of both figures is different because the receivers were deployed and recovered at different times. There were periodic depth changes between 12:00 to 13:00 and 14:00 to 16:00 at both receivers at position D which are shown by ellipsed region. The depth data in Fig. 3 (top panel) show that the receiver at 60 m was few meters shallower and deployed between 56 - 57 m.

Fig. 4 shows the water temperature data obtained at position D (top panel) and position C (bottom panel) during the measurement time. There is a significant temperature difference at both depths at position D. The temperature at the deeper receiver at position D drops by 1 degree between 14:30 and 16:00 which is the same time of depth variation in Fig. 3 (top panel). There is no significant variation in the temperature data along time at position C.

Different sets of acoustic signals were transmitted during the experiment. Chirp signals were transmitted for channel IR estimation and Binary phase shift keying (BPSK) modulated data signals were transmitted. In this paper, the chirps and BPSK data signals between 14:11 and 14:20 are analyzed. The specifications of the signals are illustrated in table 1. Table 2 shows the transmitted data sequence. During each minute, there were 15 s of chirp signals transmission, 40 s of data transmission and 5 s of silence time. The duration of each chirp signal was 0.1 s with the silence of 0.2 s so 50 chirps were transmitted each minute. The same sequence was transmitted for 9 min.

III. THEORETICAL BACKGROUND

This section provides the theoretical background of this work. The time variability in the channel IR is due to source and/or receiver and surface variations which induces Doppler effects

TABLE 1. Signal specifications.

Central Frequency (Hz)	8500
Sampling Frequency (Hz)	44100
Frequency band (data) (Hz)	7000 - 10000
Modulation	BPSK
Frequency band (Chirp) (Hz)	6320 - 10680
Duration of one Chirp (s)	0.1
Silence Time (s)	0.2

TABLE 2. Transmission sequence.

Signal Type	Chirp	BPSK	Silence
Transmission time (sec)	15	40	5

in the received signal. The Doppler effects are usually modeled as a compression/expansion of the transmitted signal.

In the underwater transmission systems, the transmitted signal reaches the receiver through different paths which are categorized as direct, surface reflected and bottom reflected paths. Fig. 5 shows a simplified diagram showing the two paths p_1 and p_2 from the source T to the receiver R. Path p_1 is the direct path from the source to the receiver while path p_2 is the surface reflected path. Considering only the surface induced motion, path p_1 is affected by the up-down movement of the surface suspended receiver and the range movement of the source. Path p_2 is directly affected by the surface motion in addition to the source-receiver motion. In Fig 5, V_T, V_R and V_S are the velocity vectors at the transmitting, receiving and the surface reflection points, respectively, $\hat{n}'_T$ and $\hat{n}'_R$ are the unit vectors in the directions of the propagation of the transmitted and received signal for the direct path and $\hat{n}''_T$ and $\hat{n}''_R$ are the unit vectors for the surface reflected path.

The Doppler induced in the received signal, due to these environmental variations, was given in [13] and [15] which is

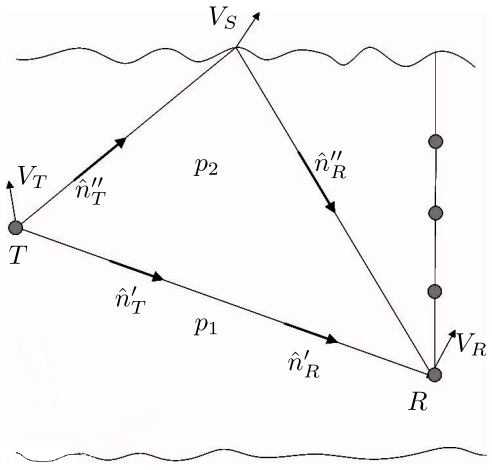

FIGURE 5. Two arriving paths from Transmitter to Receiver: Path p_1 is the direct path from the source to the receiver while p_2 is the surface reflected path. V_T, V_R, and V_S are the velocity vectors at the transmitting, receiving and the surface reflection point, respectively. $\hat{n}'_T$ and $\hat{n}'_R$ are the unit vectors in the directions of the propagation of the transmitted and received signal for the direct path while $\hat{n}''_T$ and $\hat{n}''_R$ are the unit vectors for the surface reflected path.

obtained from the compression/expansion factors ϕ' and ϕ'' for path p_1 and p_2, respectively.

$$\phi' = \frac{(V_T \cdot \hat{n}'_T - V_R \cdot \hat{n}'_R)/c}{1 - V_T \cdot \hat{n}'_T/c} + 1 \tag{1}$$

In (1) and (2), [(2) as shown at the bottom of this page], the sound speed profile c is assumed to be constant and $V_{(\cdot)} \cdot n_{(\cdot)}$ represents the projection of the velocity vectors in the path directions. The Doppler induced in path p_1 is dependent on the relative motion of the source and the receiver as given by (1). In the case of path p_2, the Doppler induced is dependent on the relative motion of source and surface, receiver and surface and source, receiver and surface as given by the three terms in the numerator in (2).

In the following, for simplicity, it is assumed that only the source is moving and v_{ip} represents the projection of V_T in the path direction of the i^{th} receiver. In such conditions, it was shown in [16] that the base-band Doppler distorted received signal at the i^{th} receiver for a single propagation path p is given by the time variable convolution

$$y_{ip}(t) = \int x(t-\tau)[g_{ip}(t,\tau)e^{-j\omega_c\tau}]d\tau \tag{3}$$

where τ represents the path delay, t is the time axis, ω_c is the carrier frequency of the band-limited transmitted signal $x(t)$ in base-band and

$$g_{ip}(t,\tau) = \frac{c - v_{ip}}{c} h_{ip}(\tau + (t-\tau)\frac{v_{ip}}{c})e^{j\omega_c(\tau + (t-\tau)\frac{v_{ip}}{c})} \tag{4}$$

is the time-variable IR in pass-band that results from the Doppler distortion of the initially propagated path p

$$g_{ip}(t=0,\tau) = h_{ip}(\tau)e^{j\omega_c\tau} \tag{5}$$

In (5), $h_{ip}(\tau)$ represents a single path, p, propagating between the source and the receiver, when the signal is assumed to be transmitted at $t = 0$ and received after the delay τ in a static environment with $v_{ip} = 0$. In (4), the path length $l_{ip}(t)$ changes with a velocity $v_{ip} = \partial l_{ip}(t)/\partial t$ due to the source motion. The ratio between this velocity and the sound speed, c, induces a delay spread in the argument of h_{ip} and a frequency spread in the form of complex exponential given in (4). The time varying IR for the single path in (4) can be generalized to a multipath channel by

$$g_i(t,\tau) = \sum_p g_{ip}(t,\tau_{ip})\delta(\tau - \tau_{ip}) \tag{6}$$

Using this in (3), the time variable signal received at the i^{th} receiver in the multipath channel is given by

$$y_i(t) = \int x(t-\tau)[g_i(t,\tau)e^{-j\omega_c\tau}]d\tau \tag{7}$$

The frequency responses (FRs) of the time variable IRs, given in (6), can be computed as

$$G_i(t,\omega) = \sum_p e^{-j\omega\tau_{ip}}[e^{j\omega t\frac{v_{ip}}{c-v_{ip}}} H_{ip}(\frac{c}{c-v_{ip}}\omega - \omega_c)] \tag{8}$$

that results from the Doppler distortion of the channel FRs when $t = 0$ and $v_{ip} = 0$, which is given by

$$G_i(t=0,\omega) = \sum_p e^{-j\omega\tau_{ip}} H_{ip}(\omega - \omega_c) \tag{9}$$

In this analysis, the velocity v_{ip} expresses the distortion by the environmental variations at the i^{th} receiver. In case of only source motion or when all the receivers experience similar environmental variations $v_{ip} \approx v_p$. This means that the distortion induced by the environmental factor is the same for all receivers. However, when the environmental variations are caused by surface variations, this approximation is not valid. Therefore, optimal performance is obtained by compensating v_{ip} separately for all receivers.

IV. TIME DIVERSITY PTR COMPENSATION

This section presents the TDpTR system for compensating the environmental variations. The proposed system is based on the pTR operator which deconvolves the channel multipath for time-invariant channels. The pTR operator is also termed as phase conjugation (PC) in frequency domain [17]. The PC operation is given by

$$P_{PC}(t,\omega) = \sum_i G_i^*(t=0,\omega)G_i(t,\omega) \tag{10}$$

where '$*$' denotes the conjugate operation, $G_i(t=0,\omega)$ is the initial FR estimate for the i^{th} receiver and $G_i(t,\omega)$ is the FR distorted by the environmental variations.

Considering that $G_i(t=0,\omega)$ and $G_i(t,\omega)$ are given by (8) and (9), respectively, and there is no channel variability ($v_{ip} = 0$), the PC operator in (10) becomes

$$\begin{aligned} P_{PC,v_{ip}=0}(t,\omega) &= \sum_i \sum_p e^{-j\omega\tau_{ip}} H_{ip}^*(\omega - \omega_c) \\ &\quad \times \sum_p e^{j\omega\tau_{ip}} H_{ip}(\omega - \omega_c) \\ &= I \sum_p |H_{ip}(\omega - \omega_c)|^2 \end{aligned} \tag{11}$$

In (11), all the paths are summed coherently which results in a channel with an enhanced single propagation path.

In the presence of environmental variability, with $v_{ip} \neq 0$, the PC operator will become

$$\begin{aligned} P_{PC,v_{ip}\neq 0}(t,\omega) = \sum_p [&H_{ip}^*(\omega - \omega_c) \\ &\times H_{ip}(\frac{c}{c-v_{ip}}\omega - \omega_c)]e^{j\omega t\frac{v_{ip}}{c-v_{ip}}} \end{aligned} \tag{12}$$

$$\phi'' = \frac{((V_T - V_S)\cdot\hat{n}''_T - (V_R - V_S)\cdot\hat{n}''_R)/c - (V_T - V_R)\cdot V_S\cdot\hat{n}''_T\cdot\hat{n}''_R/c^2}{(1 - V_S\cdot\hat{n}''_R/c)(1 - V_T\cdot\hat{n}''_T/c)} + 1 \tag{2}$$

where the paths cannot be summed coherently and the product in [·] would not result in a flat FR since the argument of G's is different. Hence, the multipath is partially compensated in the presence of environmental variations.

In this work, the time diversity of the channel is used to compensate for the environmental variations. In the conventional pTR system, the FR estimate at $t = 0$ is used to compensate for the environmental variations but it fails due to a mismatch between channel IR estimates as shown in (12). This problem is solved by transmitting multiple chirp signals before the data signal. (During the experiment, 50 chirp signals were transmitted.) The FR estimate is computed from all these 50 chirp signals and the optimal FR is selected based on the maximum output power. The optimal FR estimate is given by

$$H_{i,opt}(t,\omega) = \sum_{p} e^{-j\omega\tau_{ip}}[e^{j\omega t\frac{v'_{ip}}{c-v'_{ip}}} H_{ip}(\frac{c}{c-v'_{ip}}\omega - \omega_c)] \tag{13}$$

where v'_{ip} is the environmental variations in the FR estimate at time t. Using the optimal FR estimate, the output of the TDpTR system becomes

$$\begin{aligned} P_{TDPC}(t,\omega) &= \sum_{i} G^*_{i,opt}(t,\omega)G_i(t,\omega) \\ &\approx I\sum_{p} |H_{ip}(\frac{c}{c-v_{ip}}\omega - \omega_c)|^2 \end{aligned} \tag{14}$$

In (14), the optimal FR estimate tries to maximize the output power by matching the channel variability v_{ip} in $G_i(t,\omega)$. The optimal FR $G_{i,opt}(t,\omega)$ is selected in two different ways which are referred to as semi-TDpTR and full-TDpTR. In semi-TDpTR, it is assumed that $v_{ip} \approx v_p$. The optimal $G_{t,opt}(t,\omega)$ is selected based on this approximation. The semi-TDpTR gives the optimal performance when all the receivers are affected by the same environmental variations. In full-TDpTR, each receiver is compensated separately for different v_{ip}. The full-TDpTR gives the optimal performance when both the receivers are affected by different environmental variations.

V. TDPTR IMPLEMENTATION

The main idea of the TDpTR approach is to find the optimal channel IR which compensates for the channel variations. Fig. 6 shows the block diagram of the current implementation of the TDpTR system. The channel IRs between the source and the two receivers are represented by g_1 and g_2. During the experiment, a set of 50 chirp signals were transmitted each minute for channel IR estimation. The channel estimation from the l^{th} chirp signal at the first receiver is given by $g_1(t_l)$. The channel IRs $g(t_l)$ and $g'(t)$ represents the channel IR at different time instants. The TDpTR tries to compensate for the mismatch in $g'(t)$ using the l^{th} chirp signal. In the rest of the paper, $g(t_l)$ is referred to as the initial channel IR and $g'(t)$ is referred to as mismatched channel IR.

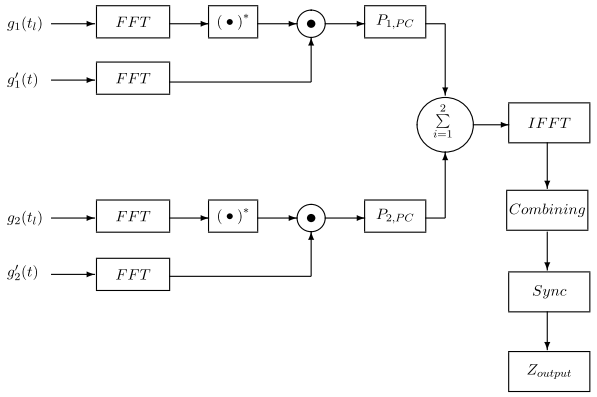

FIGURE 6. Block diagram of the TDpTR system.

The TDpTR system is implemented in the frequency domain and the FFT operation gives the FR. The $(\cdot)^*$ represents the conjugation block. The initial-conjugated FR is multiplied with the mismatched FR and summed to get the output of the phase conjugation given by (10). The *combining* block selects the optimal l^{th} chirp signal in case of TDpTR system. In case of a simple pTR system, $l = 1$ is considered for both the receivers and the channel IRs are computed from the first chirp signal. For a semi-TDpTR system, the same l^{th} chirp signal is selected for both the receivers. There are 50 chirps transmitted so the *combining* block selects the l^{th} chirp among 50 possible candidates based on the maximum output power. For full-TDpTR, all possible combinations of l are searched by the *combining* block. The l^{th} chirp is selected for each receiver separately based on the maximum output power at the *combining* block. The *sync* block compensates for the phase rotation using a known M-sequence which is transmitted at the start of the data signal.

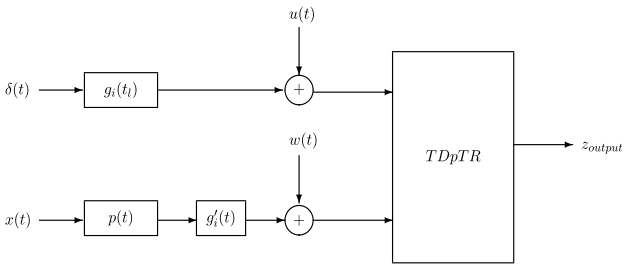

FIGURE 7. Block diagram of the TDpTR communication system.

Fig. 7 shows the block diagram of the TDpTR system when applied to underwater communications. For the purpose of applying the TDpTR for data communications, the channel IR, $g'_i(t)$, is replaced by the data signal denoted by $x(t)$ which contains the information data sequence. In the upper part of the diagram, the transmitted pulse $\delta(t)$ is passed through the channel $g_i(t)$ that represents the channel IRs during probe transmission and added with additive white Gaussian noise (AWGN), $u(t)$. In the lower part, the data signal $x(t)$ is pulse shaped by a root raised cosine signal

and convolved with the channel IRs, $g_i'(t)$, that represents the channel during the signal transmission. The noise $w(t)$ is added to the resulting signal and then fed to the TDpTR block.

VI. RESULTS AND OBSERVATIONS

This section presents the performance of TDpTR and how it compensates for the environmental variations. It is divided into two parts. In the first part, the proposed system is tested by considering the transmitted signal as a Dirac impulse. In the second part, the proposed system is extended to the communication system.

A. CHANNEL IR ANALYSIS

This section explains the performance of the proposed communication system with the FRs. The top panels in Figs. 8 and 10 show the output of the pTR operator at the position C and D by taking the inverse Fourier of the P_{PC} in (10). For the pTR operation, the first chirp ($l = 1$) is considered each minute between 14:12 to 14:20. To study the time variability over nine minutes, the FR at 14:12 is convolved with the first FR each minute.

The time variability in the channel FR is visible at both positions. The incoherent addition of the FRs results in multipath interference which is given in (12). Due to multipath interference, the main-lobe is suppressed and the side-lobes are enhanced. The main-lobe is suppressed at 14:12 and 14:18 at position C. The optimal result is obtained at 14:11 but there are small side-lobes. These side-lobes are because only two receivers are combined in the pTR operation which gives sub-optimal results. At position D, the side-lobes are high at 14:13, 14:14 and between 14:17 and 14:19. The x-axis in both figures represents the multipath spread in terms of symbols. This shows the number of adjacent symbols affected by the ISI.

The bottom panels in Figs. 8 and 10 show the channel variability during the transmission of 50 chirp signals each minute at position C and D, respectively. The channel variability is computed from pTR output in terms of multipath interference. The multipath interference is the ratio of the energy of the side-lobes to the energy of the main-lobe and expressed as $\chi(t)$. The high values of $\chi(t)$ show that the energy of the side-lobes is higher than that of the main-lobe which results in high multipath interference.

The multipath interference is high between 14:12 and 14:14, 14:15 and 14:16 and 14:18 and 14:19 at position C. These results match with the pTR output shown in Fig. 8. The multipath interference is compensated by using TDpTR. The semi-TDpTR provides a partial compensation of 2 dB between 14:13 and 14:14 and a 6 dB compensation between 14:18 and 14:19. The optimal compensation is achieved by using full-TDpTR. It compensates for the multipath interference at all three instances and provides a 4 dB gain between 14:12 to 14:14, a 4 dB gain between 14:15 and 14:16, and 14 dB gain between 14:18 and 14:19 as compared to the pTR output. Similar results are observed at position D. The multipath interference increases between 14:12 and 14:15 and 14:19 and 14:20. The semi-TDpTR provides better compensation at position D as compared to position C. It gives 5 dB gain between both 14:12 and 14:15 and 14:19 and 14:20 as compared to the pTR output. The performance is further improved by using full-TDpTR and a gain of 8 dB and 7 dB is obtained at the two instants as compared to the pTR output. Figs. 9 and 11 show the chirp signal selected for both the semi-TDpTR (top panel) and full-TDpTR (bottom panel) at positions C and D, respectively. In the case of semi-TDpTR,

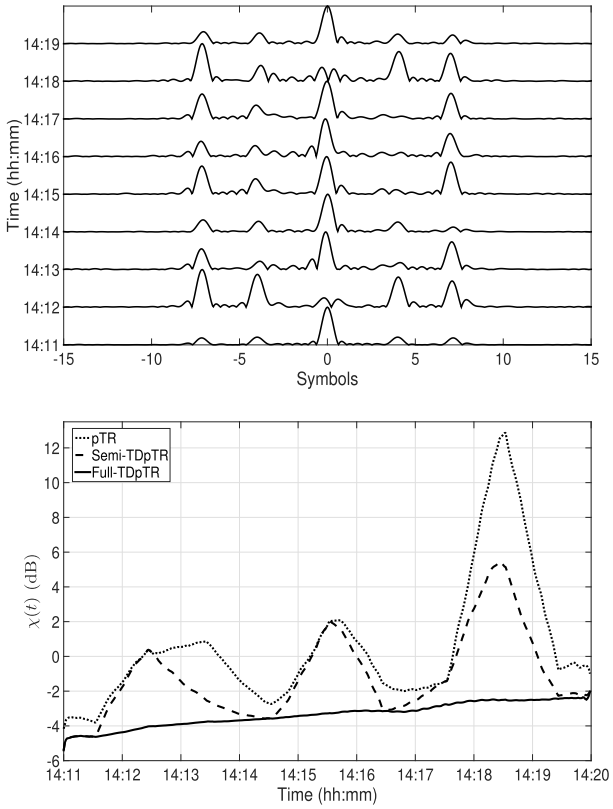

FIGURE 8. The output of the pTR operation, obtained by taking the inverse Fourier of P_{PC} in (10) at position C (top panel), the multipath interference during 15 s of chirp transmission each minute at position C (bottom panel).

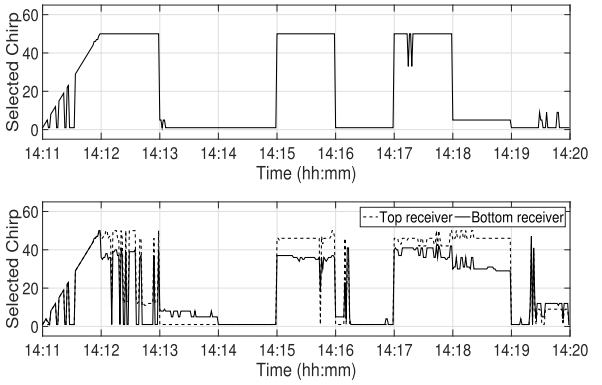

FIGURE 9. The chirps selected by the TDpTR system at position C. (a) Semi-TDpTR. (b) Full-TDpTR.

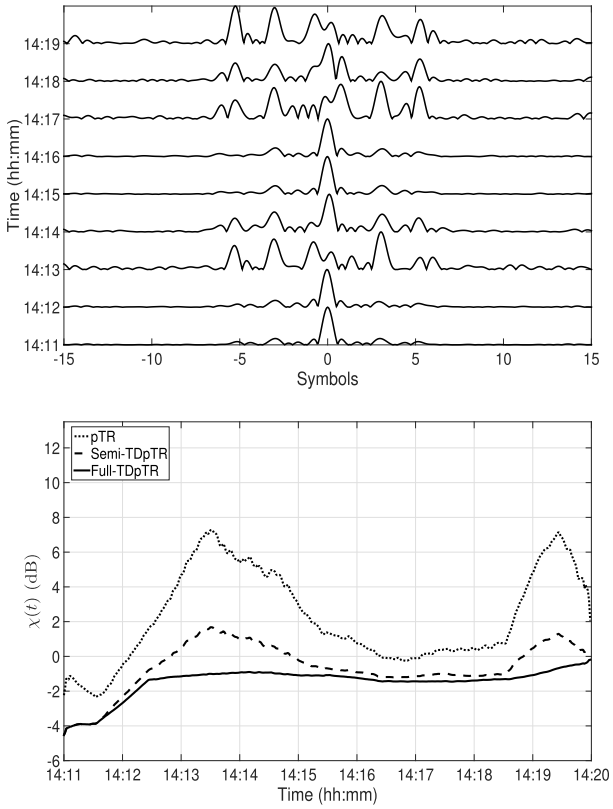

FIGURE 10. The output of the pTR operation, obtained by taking the inverse Fourier of P_{PC} in (10) at position D (top panel), the multipath interference during 15 s of chirp transmission each minute at position D (bottom panel).

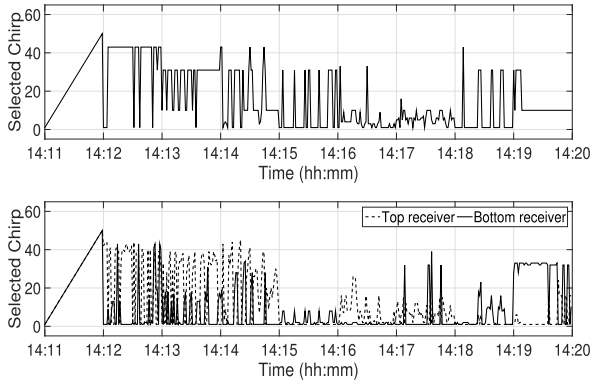

FIGURE 11. The chirps selected by the TDpTR system at position D. (a) Semi-TDpTR. (b) Full-TDpTR.

the same l^{th} chirp selected for both receivers, while different chirp signals are selected for both receivers in the case of full-TDpTR. The results show that each receiver is affected by the environmental variations in a different manner and using the FR having the same environmental variations v_p for all receivers gives a sub-optimal performance. The optimal performance is obtained by compensating both receivers with the different v_{ip}. Comparing Figs. 9 and 11 show that the channel variations are different at both positions. The channel is varying more rapidly at position D (between 14:12 and 14:15) and the full-TDpTR compensates for these variations by switching rapidly between different chirp signals at both receivers.

B. COMMUNICATION SYSTEM ANALYSIS

This section presents the performance of the proposed system in terms of MSE and BER. During the experiment, BPSK modulated information signal was transmitted for 40 s in each minute which is processed in this work. In the data processing, the information bits are segmented in 0.25 s blocks and it is assumed that the channel is constant during this time. The MSE and BER are calculated for each block and then averaged over one minute. Fig. 12 shows the performance in terms of MSE for each minute for different TR techniques at position C (top panel) and position D (bottom panel).

The performance of the pTR system degrades at position C by 3.27 dB, 3.56 dB and 3.50 dB at 14:13, 14:16 and 14:19 as compared to the performance at 14:12, respectively. The semi-TDpTR provides a gain of 0.82 dB at 14:13, 1.35 dB at 13:16 and 1.42 dB at 14:18 as compared to the pTR system. The full-TDpTR further improves the performance and provides a gain of 2.94 dB, 3.53 dB and 3.35 dB at 14:13, 14:16 and 14:18 as compared to the pTR system, respectively. However, the performance of the full-TDpTR degrades at

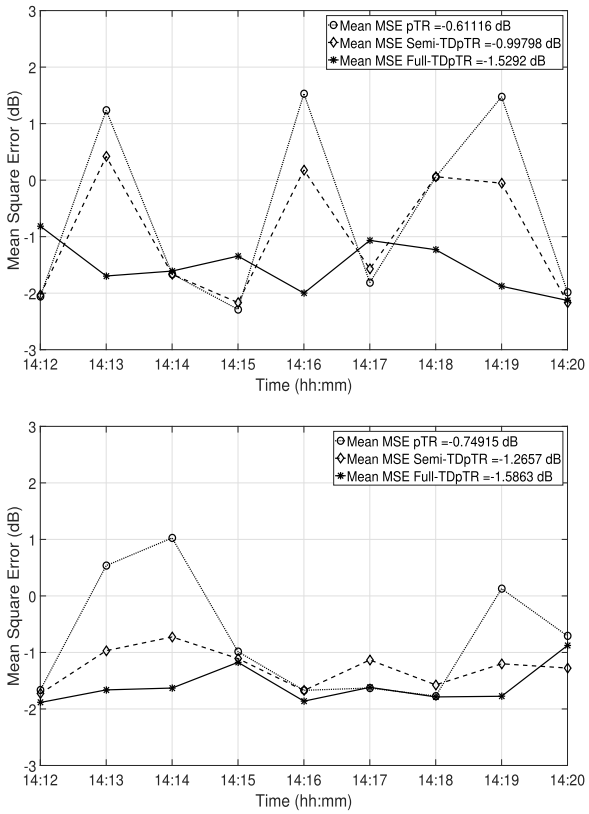

FIGURE 12. Performance comparison in terms of MSE between pTR, semi-TDpTR and full-TDpTR systems at position C (top panel) and position D (bottom panel).

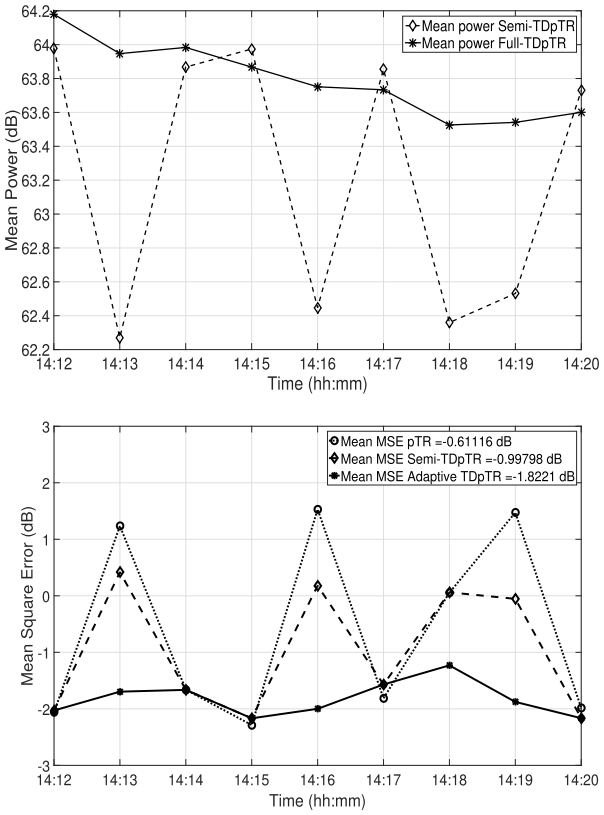

FIGURE 13. The output power for semi-TDpTR and full-TDpTR systems at position C (Top panel). The performance of the adaptive TDpTR sytem as compared to semi-TDpTR and pTR system (bottom panel).

14:12, 14:15 and 14:17. This is discussed later in this section. The objective of the TDpTR system is to compensate for the environmental variations which degrade the performance of the pTR system.

The proposed TDpTR system also gives good performance at position D. The pTR system performance degrades by 2.27 dB, 2.76 dB and 1.86 dB at 14:13, 14:14 and 14:19 as compared to the performance at 14:12, respectively. The semi-TDpTR gives a gain of 1.51 dB, 1.76 dB, and 1.33 dB as compared to pTR system at 14:12, 14:13 and 14:19, respectively. The full-TDpTR system further improves the performance by providing a gain of 2.2 dB, 2.66 dB, and 1.91 dB at 14:12, 14:13 and 14:19 as compared to pTR system. It is interesting to observe that the performances of both semi-TDpTR and full-TDpTR systems are identical at 14:12, 14:15, 14:16 and 14:18 where the channel variations are minimal. This shows that TDpTR system uses the channel diversity to compensate for the channel variations.

Tables 3 and 4 show the performance in terms of BER at position C and position D, respectively. The semi-TDpTR

TABLE 3. Performance in terms of BER at position C.

Time	BER (%)		
	pTR	Semi-TDpTR	Full-TDpTR
14:13	57.7	39.5	29.9
14:16	66.1	42.1	26.9
14:19	59.2	37.1	26.7

TABLE 4. Performance in terms of BER at position D.

Time	BER (%)		
	pTR	Semi-TDpTR	Full-TDpTR
14:13	47.3	29.9	26.0
14:14	56.1	31.3	26.3
14:19	43.9	27.7	24.6

gives a gain of 18.2 %, 24.0% and 22.1 % and full-TDpTR gives a gain of 27.8 %, 39.2 % and 32.5 % at 14:13, 14:16 and 14:19 as compared to pTR at position C, respectively. Similarly, a gain of 17.4 %, 24.8 % and 16.2 % is achieved by semi-TDpTR and a gain of 21.3 %, 29.8 % and 19.3 % is achieved by full-TDpTR as compared to pTR at 14:13, 14:14 and 14:19, respectively.

The performance of the full-TDpTR system degrades at 14:12, 14:15 and 14:17 at position C, which shows the limitation of the proposed system. In order to understand the degradation of the performance, the output power of the system is studied for semi-TDpTR and full-TDpTR, which is given by (14). The output power shows the mismatch between the channel IR estimate and the channel IR during data transmission. The difference in the output power between the semi-TDpTR and full-TDpTR shows that there is a room for improvement using the diversity gain provided by full-TDpTR. The top panel in Fig. 13 shows the mean output power every minute for semi-TDpTR and full-TDpTR at position C. The full-TDpTR system provides a gain of 1.68 dB, 1.30 dB and 1.01 dB at 14:13, 14:16 and 14:19, respectively. This gives a gain in terms of MSE. However, the difference in the output power of full-TDpTR and semi-TDpTR is 0.2 dB, -0.1 dB and -0.1 dB at 14:12, 14:15 and 14:19. As a result of that, the full-TDpTR fails to provide any gain in the MSE. The performance of pTR system is very good at 14:12, 14:15 and 14:17 which shows that the channel variations are minimal, therefore, full-TDpTR fails to provide any diversity gain. An adaptive-TDpTR (ATDpTR) is implemented to compensate for this performance loss which selects the optimal scheme between semi-TDpTR and full-TDpTR based on the output MSE. The bottom panel of Fig. 13 shows the performance of the ATDpTR system. The ATDpTR system keeps the gain of the semi-TDpTR system at 14:12, 14:15 and 14:17 and that of full-TDpTR at the rest of the time instants.

VII. CONCLUSION

The paper presents an improved version of pTR system named TDpTR which uses the time diversity of the underwater channel to compensate for the environmental variations. The proposed system is tested on the experimental data from the TrondheimFjord. During the experiment, acoustic signals were transmitted to two different receiver positions. The performance of the pTR system degrades due to strong channel variations. The proposed TDpTR system compensates for these channel variations. Two versions of TDpTR are presented in this paper, semi-TDpTR, and full-TDpTR.

The semi-TDpTR provides partial compensation in case of strong channel variations but gives better performance when the channel variations are minimal. However, the full-TDpTR provides better compensation in case of strong channel variations but fails to provide optimal performance in case of minimal channel variations. An adaptive TDpTR system is also proposed which provides the optimal solution according to the channel variations.

REFERENCES

[1] W. A. Kuperman, W. S. Hodgkiss, H. C. Song, T. Akal, C. Ferla, and D. R. Jackson, "Phase conjugation in the ocean: Experimental demonstration of an acoustic time-reversal mirror," *J. Acoust. Soc. Amer.*, vol. 103, no. 1, pp. 25–40, 1998.
[2] J. S. Kim, H. C. Song, and W. A. Kuperman, "Adaptive time-reversal mirror," *J. Acoust. Soc. Amer.*, vol. 109, no. 5, pp. 1817–1825, 2001.
[3] G. F. Edelmann, W. S. Hodgkiss, S. Kim, W. A. Kuperman, H. Song, and T. Akal, "Underwater acoustic communication using time reversal," in *Proc. MTS/IEEE Conf. (OCEANS)*, vol. 4, Nov. 2001, pp. 2231–2235.
[4] M. Stojanovic, J. A. Catipovic, and J. G. Proakis, " Reduced-complexity spatial and temporal processing of underwater acoustic communication signals," *J. Acoust. Soc. Amer.*, vol. 98, no. 2, pp. 961–972, 1995.
[5] D. Rouseff, "Intersymbol interference in underwater acoustic communications using time-reversal signal processing," *J. Acoust. Soc. Amer.*, vol. 117, no. 2, pp. 780–788, 2005.
[6] J. C. Preisig, "Performance analysis of adaptive equalization for coherent acoustic communications in the time-varying ocean environment," *J. Acoust. Soc. Amer.*, vol. 118, no. 1, pp. 263–278, 2005.
[7] M. Stojanovic, "Retrofocusing techniques for high rate acoustic communications," *J. Acoust. Soc. Amer.*, vol. 117, no. 3, pp. 1173–1185, 2005.
[8] T. H. Eggen, A. B. Baggeroer, and J. C. Preisig, "Communication over Doppler spread channels. Part I: Channel and receiver presentation," *IEEE J. Ocean. Eng.*, vol. 25, no. 1, pp. 62–71, Jan. 2000.
[9] T. H. Eggen, J. C. Preisig, and A. B. Baggeroer, "Communication over Doppler spread channels. II. Receiver characterization and practical results," *IEEE J. Ocean. Eng.*, vol. 26, no. 4, pp. 612–621, Oct. 2001.
[10] A. Song, M. Badiey, H. C. Song, W. S. Hodgkiss, M. B. Porter, and T. K. Group, "Impact of ocean variability on coherent underwater acoustic communications during the kauai experiment (kauaiex)," *J. Acoust. Soc. Amer.*, vol. 123, no. 2, pp. 856–865, 2008.
[11] A. Silva, "Environmental-based underwater communications," Ph.D. dissertation, Inst. Superior Tecnico da Univ. Tecnica de Lisboa, Lisbon, Portugal, 2009.
[12] H. C. Song *et al.*, "Spatial diversity in passive time reversal communications," *J. Acoust. Soc. Amer.*, vol. 120, no. 4, p. 2067, 2006.
[13] S. Ijaz, A. J. Silva, O. C. Rodríguez, and S. M. Jesus, "Doppler domain decomposition of the underwater acoustic channel response," in *Proc. IEEE Conf. (OCEANS)*, Santander, Spain, Jun. 2011, pp. 1–7.
[14] S. M. Jesus, S. I. Siddiqui, and A. Silva, "Path specific doppler compensation in time-reversal communications," *J. Acoust. Soc. Amer.*, vol. 137, no. 4, pp. EL300–EL306, 2015.
[15] L. J. Ziomek, *Fundamentals of Acoustic Field Theory and Space-Time Signal Processing*. Boca Raton, FL, USA: CRC Press, 1995.
[16] A. Silva, O. Rodríguez, F. Zabel, J. Huilery, and S. M. Jesus, "Underwater acoustic simulations with a time variable acoustic propagation model," in *Proc. 10th Eur. Conf. Underwater Acoust.*, vol. 2, Jul. 2010, pp. 989–996.
[17] D. Jackson and D. Dowling, "Phase conjugation in underwater acoustics," *J. Acoust. Soc. Amer.*, vol. 89, pp. 171–181, Apr. 1991.

SALMAN I. SIDDIQUI received the B.E. degree in telecommunication from the National University of Science and Technology Pakistan, in 2009, and the M.Sc. degree in electronics and telecommunication from the University of Algarve Portugal, in 2012. He is currently pursuing the Ph.D. degree with the Department of Electronic Systems, Norwegian University of Science and Technology. He was a Research Associate in different European and National projects with SIPLAB, University of Algarve, from 2009 to 2013. His research interests include underwater acoustic communications, underwater channel modeling, and signal processing for underwater communications.

HEFENG DONG received the B.Sc. degree in physics and the M.Sc. degree in theoretical physics from Northeast Normal University, China, in 1983 and 1986, respectively, and the Ph.D. degree in geoacoustics from Jilin University, China, in 1994. She was a Lecturer, from 1986 to 1994, and an Associate Professor, from 1995 to 2000, in physics with Northeast Normal University, China. She was a Visiting Scholar, from 1999 to 2000, and a Postdoctoral Fellow, from 2000 to 2001, with the Norwegian University of Science and Technology, Trondheim, Norway. She was a Research Scientist with SINTEF Petroleum Research, Trondheim, from 2001 to 2002. Since 2002, she has been a Professor in acoustic remote sensing with the Norwegian University of Science and Technology, Trondheim. She had sabbatical leave with the Underwater Acoustics Laboratory, University of Victoria, Victoria, BC, Canada, from 2008 to 2009, and the College of Earth, Ocean, and Environment, University of Delaware, USA, from 2014 to 2015. Her research interests include wave propagation modeling, geoacoustic inversion, passive acoustics, and signal processing in ocean acoustics and underwater acoustic communications.